Continual injection of photoinduced electrons stabilizing surface plasmon resonance of non-elemental-metal plasmonic photocatalyst CdS/WO$_{3-x}$ for efficient hydrogen generation

Zaizhu Lou[a], Mingshan Zhu[a], Xianguang Yang[a], Yao Zhang[a], Myung-Hwan Whangbo[b,c,d], Baojun Li[a,*], Baibiao Huang[b,*]

[a] Guangdong Provincial Key Laboratory of Optical Fiber Sensing and Communications, Institute of Nanophotonics, Jinan University, Guangzhou, 511443, China
[b] State Key Lab of Crystal Materials, Shandong University, Jinan, 250100, China
[c] Department of Chemistry, North Carolina State University, Raleigh, NC, 27695-8204, USA
[d] State Key Laboratory of Structural Chemistry, Fujian Institute of Research on the Structure of Matter (FJIRSM), Chinese Academy of Sciences (CAS), Fuzhou, 350002, China

ARTICLE INFO

ABSTRACT

To remedy the instability problem of the non-elemental-metal (NEM) plasmonic photocatalyst WO$_{3-x}$ in aqueous solution, a novel strategy of photoinduced electron injection was applied to construct CdS/WO$_{3-x}$ heterostructures by growing WO$_{3-x}$ on semiconductor CdS nanowires. Under visible/near-infrared light irradiation, the NEM plasmonic CdS/WO$_{3-x}$ nanowires are highly stable and exhibit a much higher activity (1.60 mmol g^{-1} h^{-1}) than do plasmonic WO$_{3-x}$ (negligible amount) and semiconductor CdS (0.53 mmol g^{-1} h^{-1}) in hydrogen generation. Wavelength dependent photocatalytic performance and Single-particle PL study demonstrate that photo-excited electrons on CdS continually inject into conduction band of WO$_{3-x}$, so that the surface plasmon resonance (SPR) of the NEM plasmonic photocatalyst WO$_{3-x}$ is sustained while hot electrons generated by the SPR excitation are consumed for hydrogen generation.

1. Introduction

Surface plasmon resonance (SPR) refers to electron oscillation induced by an oscillating external electromagnetic field (e.g., visible light) on the surface of noble metal nanoparticles (NPs) [1,2], which has applications in optical device [3,4], biological sensor [5,6], cancer therapy[7,8] and surface enhanced Raman scattering [9,10]. Recently, with intense visible light response, SPR was utilized to enhance visible-light-driven photocatalysis for water splitting, artificial photosynthesis and pollution decomposition [11–16]. However, the high cost of noble metals inhibit large scale applications of traditional plasmonic photocatalysts. Thus, as potential substitutes for plasmonic noble metals, non-elemental-metal (NEM) plasmonic NPs attracted attention to find that metal oxides/sulfides with heavy doping exhibit SPR phenomenon [17,18]. MoO$_{3-x}$ NPs were first reported to a NEM plasmonic catalyst to accelerate ammonia borane dehydrogenation [19–22]. The NEM plasmonic WO$_{3-x}$ nanowires and Cu$_{2-x}$S NPs have been applied in photothermal therapy and organic synthesis [23,24]. Recently, NEM plasmonic materials were found to promote plasmonic photocatalytic hydrogen generation under visible and near-infrared (NIR) light

irradiation [25]. However, recycling experiments reveal that the SPR of NEM plasmonic photocatalysts is unstable in aqueous solution.

Among various NEM plasmonic materials, WO$_{3-x}$ and MoO$_{3-x}$ are interesting because it is simple to prepare them and they exhibit an intense SPR in the visible/NIR region [26,27]. The electrons in the conduction band of WO$_{3-x}$ arise from the oxygen vacancies, which are typically generated by the chemical reduction during the synthesis [28]. As in the case noble-metal NPs, the free electrons (i.e., the conduction band electrons) of WO$_{3-x}$ can be excited by SPR to become hot electrons for the hydrogen generation [25]. However, the oxygen vacancies of WO$_{3-x}$ are easily removed in aqueous solution, hence reducing the efficiency of the plasmonic photocatalysis [29]. In addition, as the free electrons are excited to become hot electrons, the associated decrease in the number of the free electrons weakens the SPR. To boost hot electron generation and make stable NEM plasmonic photocatalyts for hydrogen generation, it would be necessary to continuously inject photogenerated electrons into NEM plasmonic NPs. Recently, the SPR of Cu$_{2-x}$S was reported to be reversible by the electron transfer from photo-excited polymers [30]. Then, in a semiconductors/WO$_{3-x}$ heterostructure, the SPR of the NEM plasmonic WO$_{3-x}$ can be made stable

if the photogenerated electrons in the semiconductor can be continuously injected into WO_{3-x}.

In this work, a novel strategy was used to construct stable NEM plasmonic photocatalysts. Heterostructural CdS/WO_{3-x} nanowires were synthesized by in-situ growth of WO_{3-x} on the semiconductor CdS nanowires, which exhibit a strong SPR absorption in the visible/NIR region. The CdS/WO_{3-x}-10 sample, where the designator "10" refers to the volume (10 mL) of the $W(CO)_6$ precursor solution used in synthesis (see below), has the photocatalytic hydrogen generation rate of $1.60\,mmol\,g^{-1}\,h^{-1}$, much higher than that of WO_{3-x} (negligible amount), and three times higher than that of CdS ($0.53\,mmol\,g^{-1}\,h^{-1}$). Single-particle photoluminescence (PL) study demonstrates that the photogenerated electrons in CdS are injected into WO_{3-x}, and the light-frequency-dependent hydrogen generation shows that the hot electrons of WO_{3-x} excited by the SPR are responsible for the photocatalytic hydrogen generation. Thus, why CdS/WO_{3-x} is highly stable and efficient in hydrogen generation under visible/NIR irradiation is explained by a mechanism in which the photogenerated electrons in the semiconductor CdS are continually injected into the NEM plasmonic catalyst WO_{3-x} to sustain its SPR.

2. Experimental

2.1. Chemicals

All reagents were of analytical grade. Thiourea (CH_4N_2S), cadmium acetate dehydrate ($C_4H_6CdO_4\cdot2H_2O$), ethylenediamine ($C_2H_8N_2$), hexacarbonyltungsten ($W(CO)_6$), lactic acid, ethanol were purchased and used without any further purification.

2.2. Synthesis of CdS nanowires

CdS nanowires were synthesized by following the reported method [31]. 1.2 g of $C_4H_6CdO_4\cdot2H_2O$ and 1.13 g of thiourea were dispersed in 80 mL $C_2H_8N_2$ under constant stirring for 1 h. After that, the mixture solution was transferred into Teflon autoclave (100 mL) and heated at 180 °C for 72 h. Finally, CdS nanowires were obtained after centrifugal separation, washed with ethanol and water for three times, and dried in oven at 60 °C for 12 h.

2.3. Synthesis of CdS/WO_{3-x} heterostructures

In a typical procedure, 1 g of $W(CO)_6$ powder was dissolved into 1L ethanol under constant stirring, and a yellow solution was obtained as the precursor solution. Then, CdS nanowires (5 mg) were suspended in the 10 mL precursor solution and then 15 mL ethanol was added under ultrasonication for 20 min. Subsequently, the solution was transferred to a 50 mL Teflon-lined stainless steel autoclave, heated up to 180 °C and kept for 12 h, then cooled down to room temperature. The green color samples were separated via centrifugation, washed with ethanol three times, and dried in oven at 60 °C for 12 h. Different samples were synthesized by following the above process using different volumes of $W(CO)_6$ precursor solution. Pure WO_{3-x} nanowires were obtained without adding CdS in above process.

2.4. Photocatalytic hydrogen generation test

In a typical process of photocatalytic reaction, 2 wt% Pt was loaded on CdS/WO_{3-x} as cocatalyts for photocatalytic hydrogen generation. Then, 3 mg of CdS/WO_{3-x} (2 wt% Pt) were dispersed into mixed solution of 4 mL Milli-Q water and 1 mL lactic acid, then was sealed with a rubber stopper in a tube, and degassed for 15 min using argon. Then, the tube was irradiated under visible-NIR light (300 mW) with magnetic stirring at room temperature. A 420 nm cutoff filter was used to remove UV light. Hydrogen evolution was detected by using gas chromatograph equipped with an MS-5A column and a thermal conductivity detector.

Different light-cutoff filters (400, 600, 720 nm) were used to investigate the hydrogen generation under different light irradiation.

2.5. Characterization

Single-particle PL images and spectra of samples were recorded by laser scanning confocal microscopy (510 META DUO SCAN, CARL ZEISS). The samples were excited through a 63 × oil-immersion lens using a circular-polarized 405-nm laser with power of 10 μW, and data of PL images and spectrum were collected. Finally, images and spectrum were analyzed by using a personal computer. TEM and HR-TEM measurements were carried out on JEOL-2100 operated at 100 kV and JEM-3000F operated at 300 kV (JEOL). SEM and EDS measurements were carried out on Hitachi SU8010 operated at 10 kV. Extinction spectra were measured by Shimadzu UV-3600 UV-VIS-NIR spectrophotometer.

3. Results and discussion

Heterostructural CdS/WO_{3-x}-10 nanowires were synthesized using the methods of our previous work [26]. Pure CdS are nanowires (Fig. S1) with smooth surface, 50–100 nm in width and micrometers in length. The prepared WO_{3-x} consists of bundles (Fig. S2) of aggregated nanowires with 2 nm in width and 20–30 nm in length. The transmission electron microscopy (TEM) images of the heterostructures show that the WO_{3-x} bundles grow along the CdS nanowires (Fig. 1a, b, e). The high resolution TEM (HR-TEM) images (Fig. 1c and d) reveal that the interplanar spacings in the bundles and nanowires are 0.380 and 0.335 nm, corresponding to (010) of $W_{18}O_{49}$ and (002) of CdS, respectively. The locations of the WO_{3-x} and CdS parts are easily recognized by the distributions of the elements W (red), S (green) and Cd (blue) in the energy dispersive x-ray spectroscopy (EDS) images (Fig. 1f–h). The EDS profile (Fig. 1i) clearly shows that the surface of the CdS nanowire is covered with WO_{3-x}. A quantitative analysis of the EDS spectrum shows that the molar ratio of WO_{3-x} to CdS in the CdS/WO_{3-x}-10 nanowires is of 1:2.7. The XRD patterns (**Fig. S3**) further confirm the chemical composition and the crystal structures of the as-prepared CdS/WO_{3-x}-10 nanowires. The composition of heterostructures is easily tuned by changing the volume of the $W(CO)_6$ precursor solution used in the synthesis. When 5 mL of the solution was used, WO_{3-x} nanowires with 10 nm in width and 100 nm in length grew along the CdS nanowires (CdS/WO_{3-x}-5) (Fig. S4). As the volume of the precursor solution increased, WO_{3-x} nanowires aggregated together to become bundles and some parts grew outside the CdS nanowires (Fig. S4c–f). As the volume is further increased to 25 mL, most surfaces of CdS nanowires were covered by WO_{3-x} bundles with many parts stretching outside (Fig. S4g–h). Heterostructures of different morphologies were further confirmed by scanning electron microscopy (SEM) images (Fig. S5). The molar ratios of WO_{3-x} to CdS in the CdS/WO_{3-x} heterostructures measured by EDS are 1:4.2, 1:2.7, 1:2.0 and 1:1.23 for CdS/WO_{3-x}-5, CdS/WO_{3-x}-10, CdS/WO_{3-x}-15 and CdS/WO_{3-x}-25, respectively.

The optical properties of the heterostructures were investigated by diffuse reflection spectroscopy (DRS). Pure WO_{3-x} prepared by $W(CO)_6$ ethanol solution has numerous oxygen vacancies, leading to a strong and broad SPR absorption in the visible/NIR region (Fig. 2a) [32]. Pure CdS nanowires show the absorption edge at 520 nm [30]. The CdS/WO_{3-x} heterostructures exhibit a broad visible/NIR absorption attributed to the SPR of the WO_{3-x} as well as the absorption of CdS nanowires. The chemical states of the elements in CdS/WO_{3-x} were analyzed by x-ray photoelectron spectroscopy (XPS) (Fig. S6). The W peaks of the XPS spectrum are divided into two groups, namely, the $4f_{5/2}$ and $4f_{7/2}$ peaks (37.89 and 35.86 eV) of W^{6+} and those (36.49 and 34.40 eV) of W^{5+}, revealing the presence of abundant O vacancies [29]. The W peaks of WO_{3-x} (Fig. S7) for the W^{5+} state (36.3 and 34.3 eV) are lower in energy than those of CdS/WO_{3-x}, which implies that there
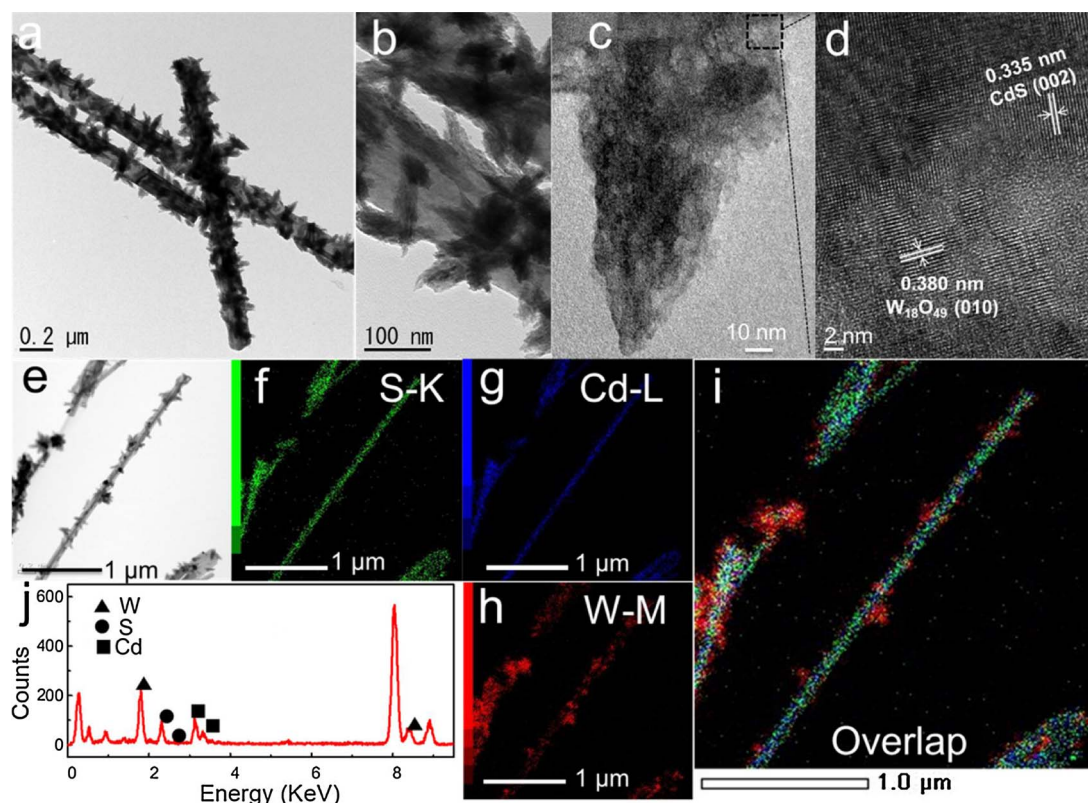
Fig. 1. (a, b, e) TEM images and (c, d) HR-TEM images of CdS/WO_{3-x}-10 heterostructures. (f–i) EDS images showing the S, Cd and W atoms of CdS/WO_{3-x}-10. (j) EDS profile of CdS/WO_{3-x}-10.(For interpretation of the references to color in the text, the reader is referred to the web version of this article.)

exist strong interactions between CdS and WO_{3-x}. The DRS spectra of CdS/WO_{3-x} with different compositions (Fig. 2b) show that, with increasing the relative amount of WO_{3-x}, the SPR absorption of the heterostructure becomes strong in the > 530 nm region. When the molar ratio of WO_{3-x} to CdS becomes greater than 1:2, the SPR absorption of the heterostructure has no increase, because the most surfaces of CdS are covered by WO_{3-x}.

We estimate the photocatalytic activity of the CdS/WO_{3-x} nanowires as photocatalysts for hydrogen generation in 20 vol% lactic acid solution under the visible/NIR light irradiation (> 420 nm). As shown in Fig. 3a, CdS/WO_{3-x}-10 generates 4.8 mmol hydrogen (normalized to 1 g catalysts) in 3 h, 3 times higher than does CdS (1.6 mmol hydrogen) and much higher than does WO_{3-x} (negligible amount). The prepared CdS/WO_{3-x}-10 also exhibited much higher activity than that of reported g-C_3N_4/WO_{3-x} (2.4 mmol hydrogen normalized to 1 g catalyst) [25]. The hydrogen generation rate is observed to be 0.95, 1.6, 0.98 and 0.79 mmol $g^{-1}h^{-1}$ for CdS/WO_{3-x}-5, CdS/WO_{3-x}-10, CdS/WO_{3-x}-15 and CdS/WO_{3-x}-25, respectively (Fig. 3b). With increasing the molar ratio of WO_{3-x} to CdS in the composition of CdS/WO_{3-x}, the SPR

absorption is improved in the visible/NIR region, leading to more hot electrons generation for the hydrogen generation. Continuously increasing the ratio reduces the exposed surface of the CdS, which eventually inhibits the oxidation reaction of the photogenerated holes in CdS, resulting in a low efficiency. The recycling stability of CdS/WO_{3-x}, we kept CdS/WO_{3-x}-10 in the dark for several days after its use as a photocatalyst once. CdS/WO_{3-x}-10 generates 5.4 mmol hydrogen in 3 h after four days in the dark, and 15 mmol hydrogen in 9 h after seven days in the dark (Fig. 3c). For three consecutive photocatalytic reactions, the average hydrogen generation rate is 1.6, 1.8 and 1.7 mmol $g^{-1}h^{-1}$. All these features demonstrate the high stability and reproducible photocatalytic activity of the CdS/WO_{3-x} heterostructures. We also investigated the light-frequency dependent hydrogen generation (Fig. 3d). The hydrogen generation rate of CdS/WO_{3-x}-10 under the irradiation of UV/Vis/NIR, > 400, > 420 and > 600 nm light are 2.7, 2.4, 1.6, 0.78 mmol $g^{-1}h^{-1}$, respectively. To our surprise, under the > 600 nm light irradiation, which excites only the SPR, the CdS/WO_{3-x} nanowires exhibit a much higher efficiency for the hydrogen generation than does pure WO_{3-x}.
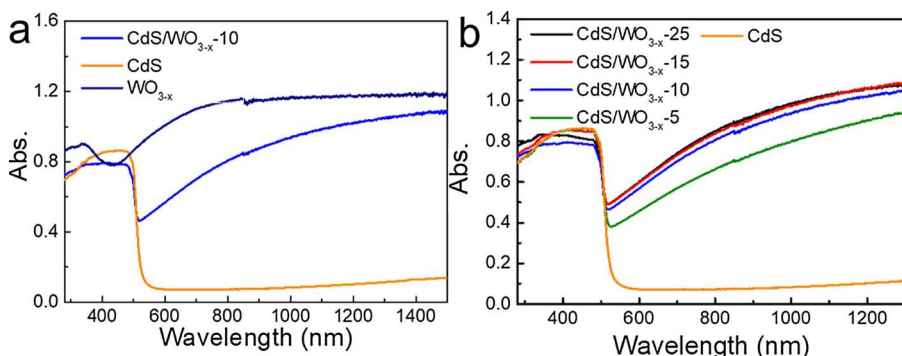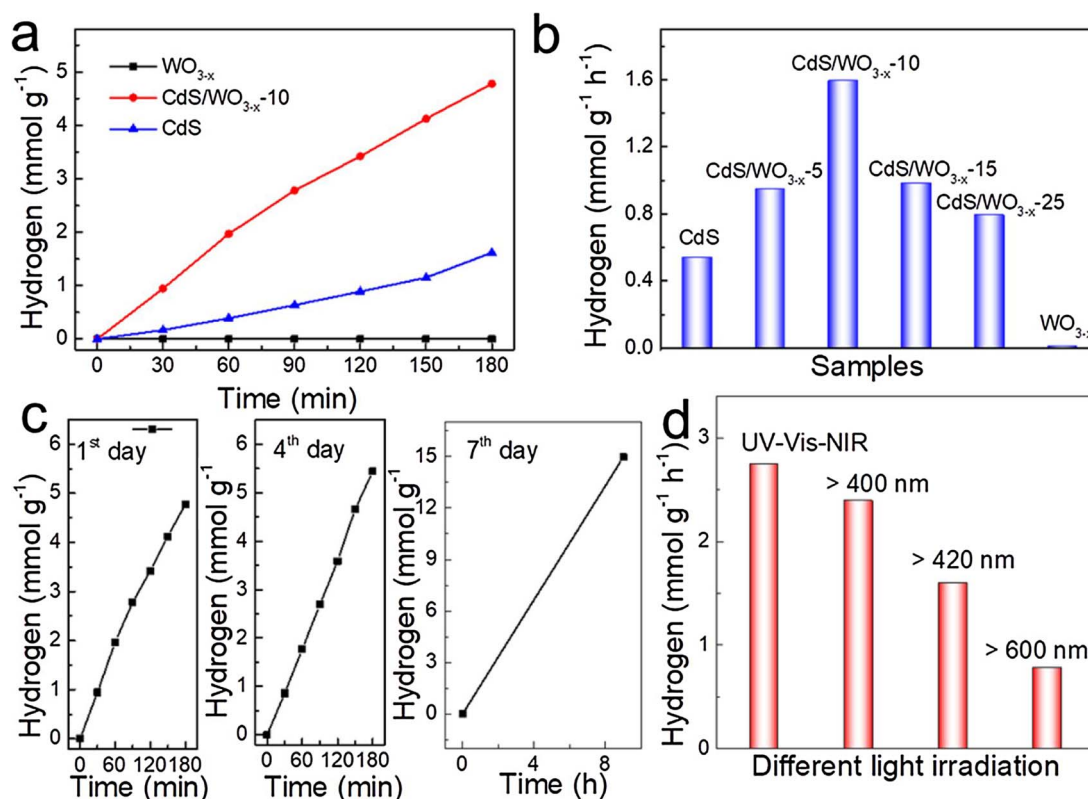

Fig. 2. (a) DRS spectra of WO_{3-x}, CdS and CdS/WO_{3-x}-10. (b) DRS spectra of the heterostructures CdS/WO_{3-x}-n heterostructures, where n = 5, 10, 15, and 25. The DRS spectrum of CdS is also shown.

Fig. 3. (a) Hydrogen generation over CdS nanowires, WO_{3-x} and CdS/WO_{3-x}-10 nanowires as photocatalysts in 20 vol% lactic solution under visible-NIR light irradiation (> 420 nm). (b) Hydrogen generation rates of CdS nanowires, CdS/WO_{3-x}-5, CdS/WO_{3-x}-10, CdS/WO_{3-x}-15, CdS/WO_{3-x}-25 and WO_{3-x} under visible-NIR light irradiation. (c) Photocatalytic reactions over CdS/WO_{3-x}-10 after keeping it four and seven days in the dark after it was used once. (d) Hydrogen generation rates of CdS/WO_{3-x}-10 under different light irradiation: UV–vis-NIR, > 400, > 420 and > 600 nm.
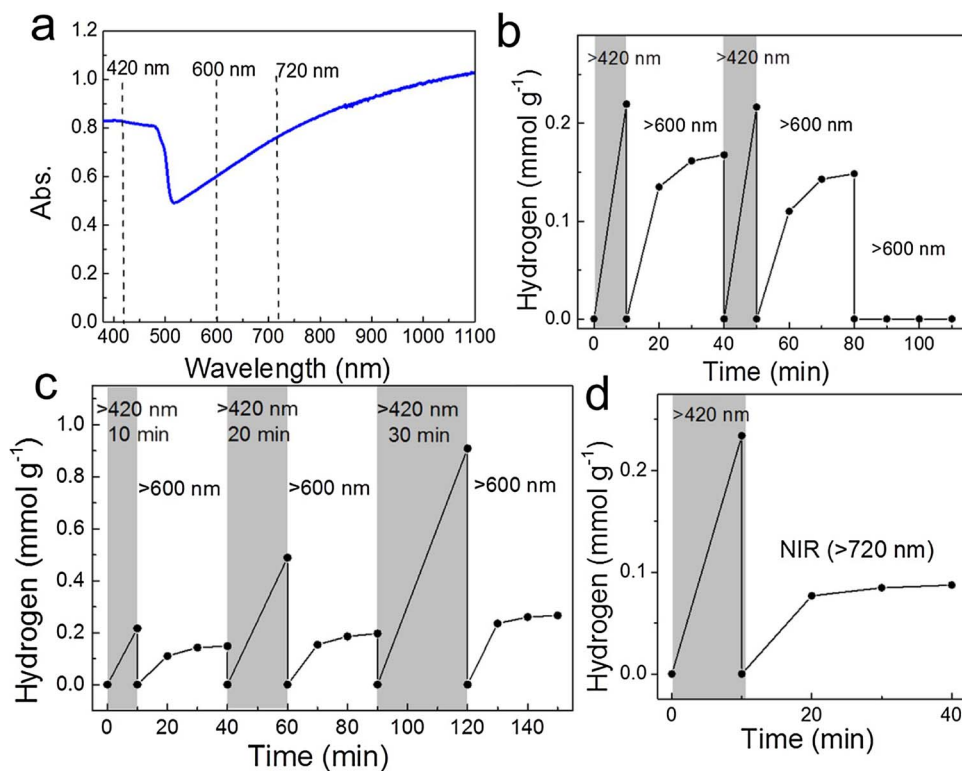
Fig. 4. (a) DRS spectrum of CdS/WO_{3-x}-10 with different regions of light irradiations to be used. (b) Photocatalytic reactions over CdS/WO_{3-x}-10 under 10 min of > 420 nm light irradiation followed by 30 min of > 600 nm light irradiation. (c) Influence of the light irradiation time on the photocatalytic activity of CdS/WO_{3-x}-10 first under > 420 nm light followed by > 600 nm. (d) Hydrogen generation over CdS/WO_{3-x}-10 under > 420 nm followed by NIR light (> 720 nm) irradiation.

To gain insight into the probable mechanism for the photocatalytic hydrogen generation by CdS/WO_{3-x} nanowires, we carried out controlled experiments with respect to the frequencies of the light irradiation (Fig. 4a). When the incident light is changed to > 600 nm after 10 min of > 420 nm irradiation, the hydrogen generation over CdS/WO_{3-x}-10 was increased with increasing the irradiation time,

with a lower generation rate (Fig. 4b). This process was repeated once and similar result was obtained. After 30 min of > 600 nm irradiation, the hydrogen generation over CdS/WO$_{3-x}$-10 nanowires became very low (Fig. 4b). Without the > 420 nm irradiation, a negligible amount of hydrogen was detected over CdS/WO$_{3-x}$-10 under > 600 nm irradiation. The color of CdS/WO$_{3-x}$-10 precipitation became dark green after the > 420 nm irradiation (Fig. S8), implying that use of the > 420 nm irradiation leads to more electrons in WO$_{3-x}$. This can be explained if we assume that the photogenerated electrons in CdS are injected into WO$_{3-x}$ and then are excited by the SPR to become hot electrons for the hydrogen generation. To probe the dependence of the electron-injection on the irradiation time under > 420 nm, we examine the hydrogen generation over CdS/WO$_{3-x}$-10 nanowires under different irradiation time (Fig. 4c). As the irradiation time increases from 10 to 30 min, the hydrogen generation rate became fast in the first 10 min under the > 600 nm irradiation and became slow after 30 min, indicating the diminished NEM plasmonic activity. A photocatalytic hydrogen generation by CdS/WO$_{3-x}$-10 nanowires was also observed under NIR irradiation (> 720 nm) (Fig. 4d), which further demonstrates that the hydrogen generation is due to the SPR of WO$_{3-x}$. Therefore, the synergetic effect between the injection of the photogenerated electrons from CdS to WO$_{3-x}$ and the stabilization of the SPR of WO$_{3-x}$ are responsible for a highly stable and efficient NEM plasmonic photocatalysis for hydrogen generation by CdS/WO$_{3-x}$.

To probe the role of CdS plays in the photocatalytic activity of the CdS/WO$_{3-x}$, we first evaluate the activity of WO$_{3-x}$ on its own. The prepared WO$_{3-x}$ was dissolved into 20 vol% lactic acid solutions for photocatalytic hydrogen generation. The visible/NIR absorption spectra (Fig. 5a) show that WO$_{3-x}$ has a wide band gap for ultraviolet (UV) absorption and a weak SPR absorption in the visible/NIR region. Thus, the visible light (> 420 nm) irradiation excites only the SPR, and no hydrogen generation was detected in the photocatalytic reaction. To increase the number of the free electrons in WO$_{3-x}$, UV light was irradiated for 1.5 h so that the SPR absorption became stronger (Fig. 5a), revealing that more free electrons are accumulated in WO$_{3-x}$. In this case, the photocatalytic hydrogen generation rate of the plasmonic WO$_{3-x}$ was measured to be nonzero but very small (i.e., 14 μmol g^{-1} h^{-1}, Fig. 5b). Clearly, the seminconductor CdS in the CdS/WO$_{3-x}$ heterostructure is crucial for photocatalytic activity of the CdS/WO$_{3-x}$.

To find experimental evidence that the photogenerated electrons in the semiconductor part of CdS are injected into the NEM plasmonic photocatalyst part WO$_{3-x}$ in the CdS/WO$_{3-x}$ heterostructures, we performed single-particle photoluminescence (PL) studies on CdS and CdS/WO$_{3-x}$ (Fig. 6) using the 405-nm laser as the light exciting source. No emission was observed from the WO$_{3-x}$ nanowires, showing no transition across the band gap from the WO$_{3-x}$ in the visible light region. The CdS nanowires exhibit a strong emission at 510 nm, and are observed in the PL image (Fig. 6a). The morphologies of CdS/WO$_{3-x}$-10 heterostructures were also observed as nanowires in the PL image (Fig. 6b), but is much darker than the PL image of CdS nanowires, most

likely because a PL quenching occurs in the heterostructures. Single-particle PL spectra clearly showed the PL quenching in Fig. 6c. The transfer of photogenerated electrons competes with their radiative decay for PL, leading to PL quenching [11,12]. The occurrence of a PL quenching in the heterostructures signifies that the photoelectron transfer from the CdS to the WO$_{3-x}$ part under visible light irradiation. From the time-resolved PL spectra of CdS and CdS/WO$_{3-x}$ (Fig. S9), their average fluorescence lifetimes are calculated to be 0.32 ns for CdS, and 0.25 ns for CdS/WO$_{3-x}$. That CdS/WO$_{3-x}$ has shorter lifetime than does CdS further confirms the transfer of the photogenerated electrons from CdS to WO$_{3-x}$.

The experimental results described above allow us to propose a probable mechanism for the NEM plasmonic photocatalysis of CdS/WO$_{3-x}$ heterostructures as described in Fig. 6d. Under visible/NIR light (> 420 nm) irradiation, the electrons in the valence band of CdS are excited to the conduction band, and are then injected into WO$_{3-x}$ with lower-lying Femi level. The hole left on the valence band of CdS reacts with electron donor (lactic acid). Due to the injection of photogenerated electrons, the number of free electrons in the conduction band of WO$_{3-x}$ is increased and hence its SPR becomes stable, and some of the free electrons are excited to become hot electrons for the hydrogen generation. The loss of electrons in WO$_{3-x}$ arising from the hydrogen generation is constantly replenished by the injection of the photogenerated electrons from CdS, leading to a stable and efficient NEM plasmonic WO$_{3-x}$ for the photocatalytic hydrogen generation.

4. Conclusions

In summary, a new strategy of photoinduced electron injection was proposed to construct stable NEM plasmonic photocatalysts for water splitting, and the heterostructure CdS/WO$_{3-x}$ was successfully prepared by combining NEM plasmonic WO$_{3-x}$ and semiconductor CdS nanowires. Sample CdS/WO$_{3-x}$-10 was demonstrated to be optimal structure for plasmonic photocatalytic hydrogen generation, which was 1.6 mmol g^{-1} h^{-1}, three times higher than that of CdS (0.52 mmol g^{-1} h^{-1}) and much higher than that of WO$_{3-x}$ under visible/NIR light irradiation. Single-particle PL study demonstrated the photoelectron generate on CdS nanowires transfer to plasmonic WO$_{3-x}$, which stabilizes its surface plasmon resonance during photocatalysis and boosts the photocatalytic hydrogen generation under visible-NIR irradiation. Our work provides a new strategy to construct highly stable and active plasmonic photocatalysts for water splitting.
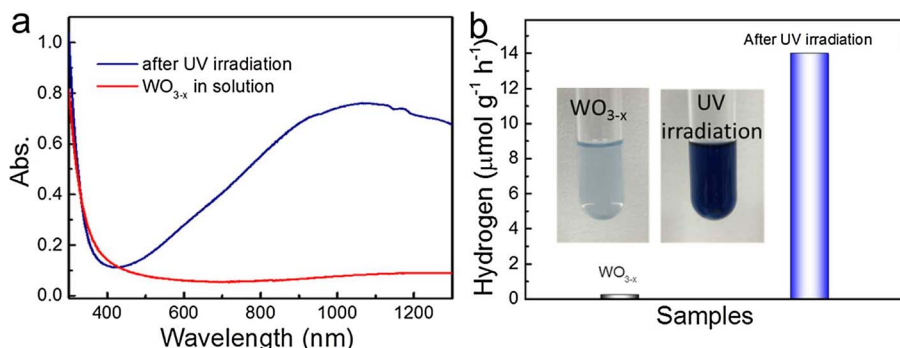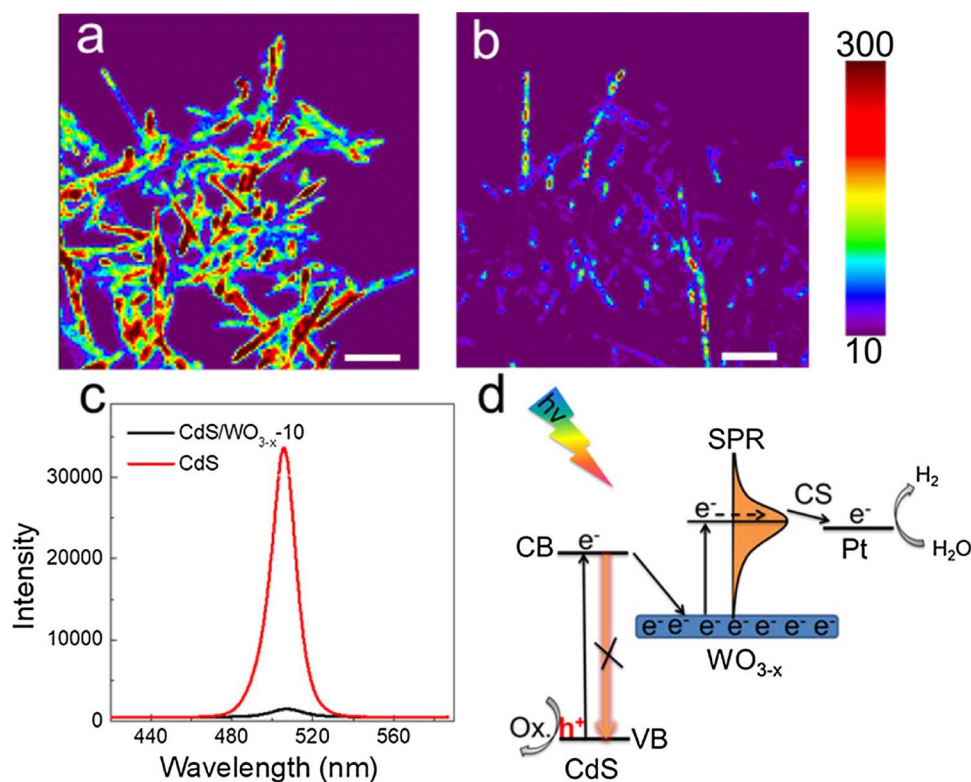
Acknowledgements

Fig. 5. (a) Visible-NIR absorption spectra and (b) photocatalytic hydrogen generation of the WO$_{3-x}$ solution before and after UV irradiation. Insert figures in b show colors of WO$_{3-x}$ solution before and after UV irradiation.

Fig. 6. Single-particle PL images of (a) CdS and (b) CdS/WO$_{3-x}$-10 nanowires. Scale bar: 1 μm. (c) Single-particle PL spectra of CdS and CdS/WO$_{3-x}$-10 nanowires. (d) Schematic diagram showing why the injection of the photogenerated electrons from the semiconductor CdS to the NEM plasmonic photocatalyst WO$_{3-x}$ stabilizes CdS/WO$_{3-x}$ and enhances its hydrogen generation.

Appendix A. Supplementary data

Supplementary data associated with this article can be found, in the online version, at https://doi.org/10.1016/j.apcatb.2017.12.023.

References

[1] C.M. Cobley, J. Chen, E.C. Cho, L.V. Wang, Y. Xia, Chem. Soc. Rev. 40 (2011) 44–56.
[2] X. Zhang, Y.L. Chen, R.S. Liu, D.P. Tsai, Rep. Prog. Phys. 76 (2013) 046401.
[3] F. Ye, M.J. Burns, M.J. Naughton, Nano Lett. 13 (2013) 519–523.
[4] M. Bahramipanah, S. Dutta-Gupta, B. Abasahl, O.J.F. Martin, ACS Nano 9 (2015) 7621–7633.
[5] J.R.L. Guerreiro, M. Frederiksen, V.E. Bochenkov, V.D. Freitas, M.G.F. Sales, D.S. Sutherland, ACS Nano 8 (2014) 7958–7967.
[6] Y.X. Lu, Y.Y. Liu, S.G. Zhang, S. Wang, S.C. Zhang, X.R. Zhang, Anal. Chem. 85 (2013) 6571–6574.
[7] N. Frazier, R. Robinson, A. Ray, H. Ghandehari, Mol. Pharm. 12 (2015) 1605–1614.
[8] Y.Y. Li, T. Wen, R.F. Zhao, X.X. Liu, T.J. Ji, H. Wang, X.W. Shi, J. Shi, J.Y. Wei, Y.L. Zhao, X.C. Wu, G.J. Nie, ACS Nano 8 (2014) 11529–11542.
[9] K.K. Liu, S. Tadepalli, L.M. Tian, S. Singamaneni, Chem. Mater. 27 (2015) 5261–5370.
[10] J.M. Nam, J.W. Oh, H. Lee, Y.D. Suh, Acc. Chem. Res. 49 (2016) 2746–2755.
[11] Z.Z. Lou, S. Kim, P. Zhang, X.W. Shi, M. Fujitsuka, T. Majima, ACS Nano 11 (2017) 968–974.
[12] Z.Z. Lou, M. Fujitsuka, T. Majima, J. Phys. Chem. Lett. 8 (2017) 844–849.
[13] Y. Shiraishi, H. Sakamoto, Y. Sugano, S. Ichikawa, T. Hirai, ACS Nano 7 (2013) 9287–9297.
[14] Y. Yoshinaga, T. Akita, I. Mikami, T. Okuhara, J. Catal. 207 (2002) 37–45.
[15] P. Wang, B.B. Huang, X.Y. Qin, X.Y. Zhang, Y. Dai, J.Y. Wei, M.H. Whangbo, Angew. Chem. Int. Ed. 47 (2008) 7931–7933.
[16] Z.Z. Lou, B.B. Huang, X.Y. Qin, X.Y. Zhang, H.F. Cheng, Y.Y. Liu, S.Y. Wang, J.P. Wang, Y. Dai, Chem. Comm. 48 (2012) 3488–3490.
[17] Q. Huang, S. Hu, J. Zhuang, X. Wang, J. Chem. Eur. 18 (2012) 15283–15287.
[18] Y. Zhao, H. Pan, Y. Lou, X. Qiu, J. Zhu, C. Burda, J. Am. Chem. Soc. 131 (2009) 4253–4261.
[19] H.F. Cheng, X.F. Qian, Y. Kuwahara, K. Mori, H. Yamashita, Adv. Mater. 27 (2015) 4616–4621.
[20] H.F. Cheng, T. Kamegawa, K. Mori, H. Yamashita, Angew. Chem. Int. Ed. 53 (2014) 2910–2914.
[21] H.B. Yin, Y. Kuwahara, K. Mori, H.F. Cheng, M.C. Wen, Y.N. Huo, H. Yamashita, J. Phys. Chem. C 121 (2017) 23531–23540.
[22] M.C. Wen, K. Mori, Y. Kuwahara, H. Yamashita, ACS Energy Lett. 2 (2017) 1–7.
[23] Z.Z. Lou, Q. Gu, Y.S. Liao, S.J. Yu, C. Xue, Appl. Catal. B: Environ. 184 (2016) 258–263.
[24] J.B. Cui, Y.J. Li, L. Liu, L. Chen, J. Xu, J.W. Ma, G. Fang, E.B. Zhu, H. Wu, L.X. Zhao, L.Y. Wang, Y. Huang, Nano Lett. 15 (2015) 6295–6301.
[25] Z.Y. Zhang, J.D. Huang, Y.R. Fang, M.Y. Zhang, K.C. Liu, B. Dong, Adv. Mater. 29 (2017) 5906–5914.
[26] Z.Z. Lou, Q. Gu, L. Xu, Y.S. Liao, C. Xue, J. Chem. Asian 10 (2015) 1291–1294.
[27] G. Song, J. Shen, F. Jiang, R. Hu, W. Li, L. An, R. Zou, Z. Chen, Z. Qin, J. Hu, ACS Appl. Mater. Interfaces 6 (2014) 3915–3922.
[28] R. Chatten, A.V. Chadwick, A. Rougier, P.J.D. Lindan, J. Phys. Chem. B 109 (2005) 3146–3156.
[29] G.C. Xi, S.X. Ouyang, P. Li, J.H. Ye, Q. Ma, N. Su, H. Bai, C. Wang, Angew. Chem. Int. Ed. 51 (2012) 2395–2399.
[30] R. Alam, M. Labine, C.J. Karwacki, P.V. Kamat, ACS Nano 10 (2016) 2880–2886.
[31] C.Y. Zhai, M.J. Sun, M.S. Zhu, K. Zhang, Y.K. Du, Int. J. Hydrogen Energy 42 (2017) 5006–5015.
[32] K. Manthiram, A.P. Alivisatos, J. Am. Chem. Soc. 134 (2012) 3995–3998.